Ban. J. Med. Phys., Vol -16, Issue -2, 2025 : 44-55

ORIGINAL ARTICLE

BANGLADESH JOURNAL OF MEDICAL PHYSICS

Journal Homepage: www.banglajolinfo/index.php/bjmp

Measurement Stability of Spectral Computed Tomography

M Rayhan Uddin[1]*, Marzieh Anjomrouz[3], Philip H Butler[1, 2, 3, 4, 5,] MARS Collaboration[1,2,3,4,5]

[1]*University of Canterbury, Christchurch, New Zealand*

[2]*MARS Bioimaging Limited, Christchurch, New Zealand*

[3]*University of Otago Christchurch, Christchurch, New Zealand*

[4]*European Organisation for Nuclear Research (CERN), Geneva, Switzerland*

[5]*Human Interface Technology Laboratory New Zealand, University of Canterbury, Christchurch, New Zealand*

ARTICLE INFO

Article history:
Received : 18 August 2025
Received in revised form : 13 September 2025
Accepted : 26 September 2025
Available online : 01 October 2025

Key words:

Spectral Computed tomography, photon-counting detector, Spectral signature, measurement error and stability.

doi: https://doi.org/10.3329/bjmp.v16i2.84806

Article Category: Diagnostic Radiology

***Corresponding author:**
M Rayhan Uddin
rayhanru2011@gmail.com

ABSTRACT

The aim of this study is a comprehensive investigation of measurement stability of MARS spectral computed tomography to evaluate the variability in the measured spectral signature of different materials and count rate capability of Medipix3RX chip. The intra and inter-scan measurement variation of the mass attenuation coefficient of different materials and the count rate capability of the Medipix3RX chip were evaluated. A repeated scan was performed using multi-contrast phantom in different MARS scanner to quantify the error of the mass attenuation coefficient of different materials. A hypothesis was made to assume how different instabilities occurred measurement variation in the spectral signature. The performance of a relative count rate of different charge summing counter was also evaluated to investigate the temporal stability of the Medipix3RX photon-counting detector. The mass attenuation profile of different composite and single materials produces scan variation in repeated measurement. The variation of the mass attenuation coefficient of composite materials was significantly higher compared to the single materials. The Bland-Altman plot shows that the linear attenuation coefficients of each voxel corresponding to each composite material produce more outlier points outside the 95% confidence interval than single materials. Relative count variation in each charge summing counter of Medipix3RX chip was observed during repeated air scan. These investigations provide useful insights into the source of variation of the MARS spectral CT system and indicate potential areas where future improvements in performance may be made.

1. Introduction

The Medipix All Resolution System (MARS) is a quantitative colour x-ray imaging modality that incorporates with the Medipix3RX photon-counting detector. The MARS imaging technology is based on counting the number of photons at multiple narrow energy bands over the entire x-ray spectrum. For this reason, it is often referred to as photon-counting or spectroscopic or multi-energy CT imaging modality [1]. The Medipix detectors are hybrid detectors consisting of a semiconductor sensor layer that is bump bonded to an electronics layer [2]. Medipix3RX is the latest version that allows simultaneous measurement of x-rays photons within up to eight energy ranges, therefore a single exposure has much more information. It has 128 × 128-pixel array per chip. Every pixel accurately counts and measures the number of photons that reach it within specified energy bands [3]. Medipix3RX detector can be adjusted in different operating mode and the choice of a particular operating mode depends on the application. For instance, the charge summing mode (CSM) provides for the improved spectroscopic capability of the detector and can be useful for soft tissue imaging. In contrast, the spectroscopic mode is associated with loss of spatial resolution with consequent effects of image quality degradation especially for procedures that require detailed morphology of the specimen [4].

Conventional CT scanners use an energy integrating detector that measures the attenuated signal over the entire x-ray spectrum, therefore all materials produce same CT number at a certain concentration. For this reason, it is not possible to separate the materials from each other [5]. Dual-energy CT able to distinguish two materials only at

two energy bins but has limitations in materials discrimination for multiple materials. Due to the use of the spectroscopic nature of Medipix3RX detector, MARS scanner can measure attenuation difference of different materials at different energy threshold in diagnostic energy range and that allows to identify and quantify different materials in a different colour. The MARS scanner plays an important role in different pre-clinical applications. The current small-bore MARS scanner has contributed to different pre-clinical areas such as monitoring the biomarker for cancer imaging, identifying unstable atherosclerosis plaque and its treatment, characterizing cartilage to identify osteoarthritis, and applications in the meat industry [6]. The recent breakthrough is the application of a human-sized to image live human patients using the MARS scanner [7].

There are many factors that can lead to observable variations in measurement of MARS spectral CT system that degrade spectral image quality. Examples of this include mechanical misalignment, inter-pixel differences, changes in detector temperature, detector instabilities, and drift in energy thresholds. These variations can severely degrade the measured spectral signal in reconstructed images. Inter-pixel variation reduces the energy resolution [8]. Geometric misalignment produces image blurring [9]. Temperature variation and detector instability affect the energy response of the Medipix3RX detector and cause threshold drifting [10]. Variation such as these, if unaccounted for, result in image artifacts in the spectrally reconstructed data.

Characterizing the sources of variability of spectral CT scanner is very important to obtain better image quality and higher sensitivity for detecting different materials. Many methods have been published for measurement variation of computed tomography systems. Among them, the work published by Toru Kobayashi *et al*. can be referred to. They evaluated the accuracy of linear attenuation coefficients using a photon-counting CT system [11]. It was found that the linear attenuation coefficient of single materials agreed with the theoretical values better than the composites materials. Tyler E. Curtis *et al.* [12], investigated the spatial and quantitative accuracy of material decomposition for mixed contrast agents. They found that the value of the root mean square (RMSE) was less than 12% of the maximum signal for each material in mixed compositions.

One of the important challenges in the development of spectral CT technology is that the location of energy thresholds. Threshold variation or drifting leads to ring artifact in the reconstructed images. Another critical challenge of the photon-counting CT is called inhomogeneity of the detector element. It is not possible to manufacture readout electronics with completely identical components. For this reason, there will be variation between detector elements that causes the changes in the energy threshold with respect detector element. Due to threshold variation, some detector elements count more photons than others and photons with the same energy can be registered in different energy bins [13].

The main aim of this study is to evaluate the stability of mass attenuation profile of different materials and count rate capability of Medipix3RX chip to investigate measurement variation on same spectral CT scanner. To address this issue, a study was conducted to characterize the measurement variation during a repeated scan of multi-contrast phantom by the spectral CT scanner. In this study, the relative count performance of different charge summing counter was also evaluated with respect to the arbitration counter to investigate threshold drifting.

2. Materials and Methods

2.1 MARS Spectral CT scanner

The current version of the MARS scanner is manufactured for small animals and human excised specimens. The maximum field of view is 100 mm in diameter and 270 mm in length. Two MARS components are an x-ray tube to generate a narrow cone beam, and a camera to detect the photons passed through the subject (e.g., an object, an excised specimen, a live or plasticized animal, or human). These components are mounted in a mechanical housing called a gantry which rotates around the subject on a fixed axis. The subject is mounted on a holder that is translated perpendicular to the gantry rotation to cover part or all of the subject during a scan shown in Fig. 1. The mass attenuation coefficient of different materials across the x-ray spectrum can be measured at different energy bins using MARS spectral CT scanner that is demonstrated in Fig. 2.

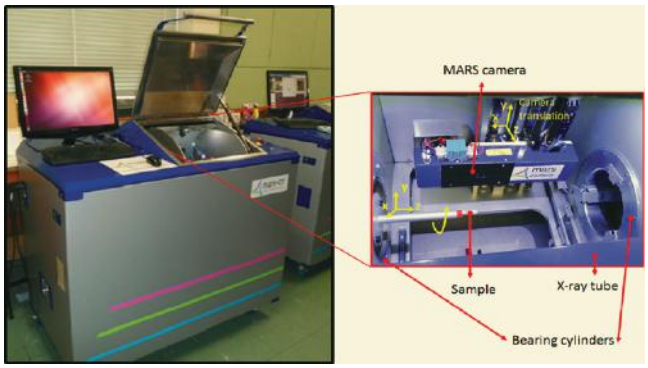

Fig. 1. A small-bore MARS spectral CT scanner. The magnified image (right) shows the x-ray tube, camera, and sample inside the gantry. The x-ray source and camera are mounted on the gantry that rotates around the subject.

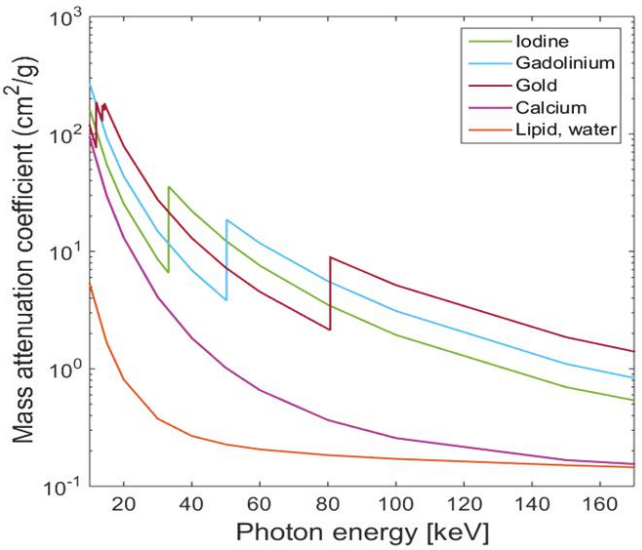

Fig. 2. Comparison of mass attenuation coefficients for iodine, gadolinium, gold, calcium, lipid and water over the x-ray spectrum of 20-120 keV.

2.2 Multi-Contrast Phantom

Multi-contrast phantom was used to measure linear attenuation of different materials. The circular shape multi-contrast phantom with a diameter of 31 mm and nine vials including different materials were inserted and the diameter of each vial was 6 mm. The vials of these phantoms with water and lipid as single materials and calcium, gadolinium, iodine, and gold as composite materials. The schematic diagram of multi-contrast phantom is depicted in Fig. 3. The composite materials are also divided into two categories of non-K-edge materials such as calcium which does not have K-edge in the diagnostic energy range. Gold, gadolinium, and iodine which has K-edge properties, as shown in Fig. 2. K-edge materials are often used as contrast agents as they enhance the visibility of fluid or structures of tissue in the body. The multi-contrast phantom consists of different material concentrations of lipid, water, 8 mg/mL and 2 mg/mL of gold, 8 mg/mL and 2 mg/mL of gadolinium, 18 mg/mL of iodine and 240 mg/mL of calcium. The reconstructed images of a phantom obtained by MARS scanner with CZT-Medipix3RX detector in different energy bins is presented in Fig. 4. The same circular shape ROI was selected for each material from the averaged images. The area of ROI was 15 mm^2.

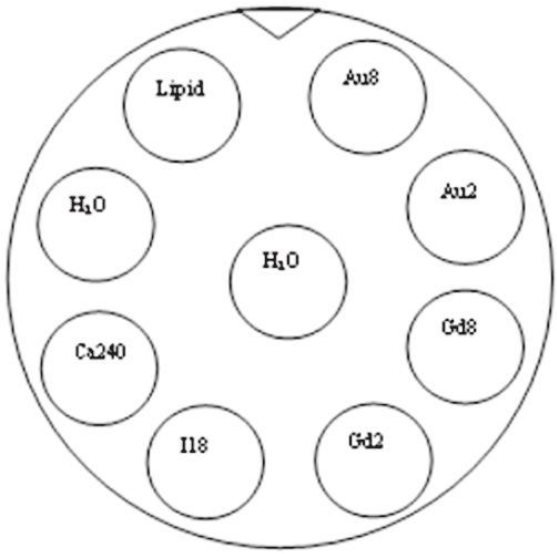

Fig. 3. Schematic diagram of multi contrast QA phantom with various concentrations (mg/mL).

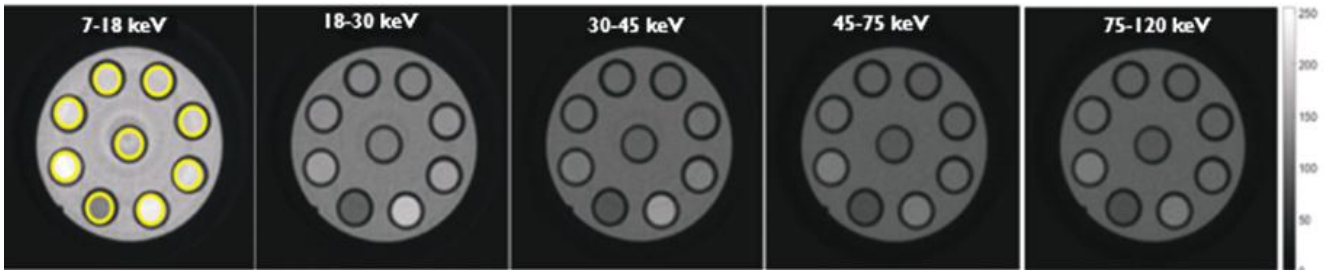

Fig. 4. Reconstructed images of a multi-contrast phantom obtained by MARS scanner with CZT-Medipix3RX detector in five energy bins. In the first image from the left, selected ROIs are also demonstrated.

2.3 Experimental Setup

2.3.1 Protocol 1: Scan of Multi-Contrast Phantom

A repeated scan was performed using a multi-contrast phantom on the MARS scanner. All the experiments were conducted using a polychromatic x-ray source (Model SB-120-700-P-CW, Source-Ray Inc, Ronkonkoma, NY). The camera used in this scanner was a Medipix3RX detector flip-bonded to 2 mm CZT. The scan parameters of this protocol included the tube voltage of 120 kVp, tube current of 13 μA, and exposure time of 300 ms, and 3.1 mm aluminium filtration. The source to object distance (SOD), and object to detector distance (ODD) and source to detector distance (SDD) was 200 mm, 50 mm and 250 mm, respectively. Five back-to-back scans of the multi-contrast phantom were taken using the same protocol on the same day. Five energy bins were set to 7-18 keV, 18-30 keV, 30-45 keV, 45-75 keV and 75-120 keV in CSM mode so that these energy ranges can identify of the K-edge. The K-edge of iodine (33.17 keV) is in the third energy bin, K-edge of gadolinium (50.24 keV) is in the fourth energy bin, K-edge of gold (80.72 keV) were targeted at 75-120 keV energy bin.

2.3.2 Protocol 2: Air Scan

Six back-to-back air scans were performed in MARS scanner that utilized a polychromatic x-ray source (Model SB-120-350-GW-157, Source ray SB-125-350.SN:157) and with a seven chip MARS camera (CZT-7x1-5.4-SN208-CZT:3RX-7chips) to evaluate count of each charge summing mode (CSM) with respect to the arbitration counter. The energy threshold was split into eight energy bins over the polychromatic x-ray spectrum (120 kVp). The chip was bonded to the CZT sensor layer and a pixel pitch of 110 μm each with eight simultaneous threshold counters, four of which utilize real-time charge summing to significantly reduce the charge sharing between contiguous pixels. The protocol was included the tube voltage of 120 kVp, tube current of 25 μA, exposure time of 100 ms, and 1.96 mm aluminum filtration. Source to object distance (SOD) and object to detector distance (ODD) was 280 mm and 200 mm respectively. Eight energy bins were set to 7 keV 22.9 keV, 42.9 keV, 54.9 keV, 70 keV, 74 keV, 77 keV, 78 keV in spectroscopic mode. Before the actual acquisition of the count rate, the x-ray tube was activated for 20 seconds to warm up for ensuring the x-ray flux output was stable.

Fig.5 shows the interior diagram of the MARS scanner during the air scan. The raw image of the seven chip MARS camera at different counters is presented in Fig. 6.

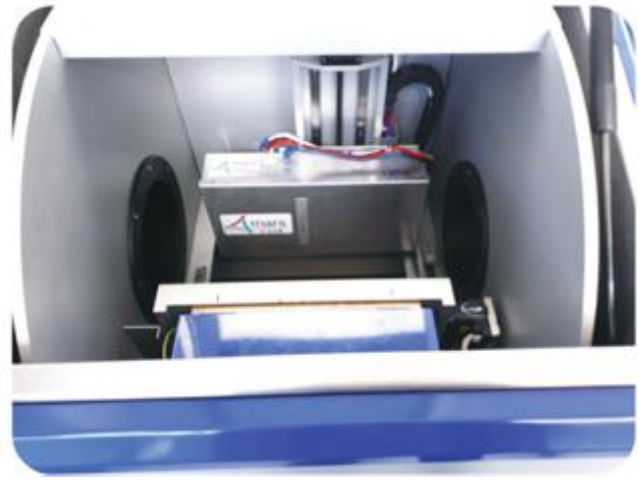

Fig. 5. Interior diagram of spectral CT scanner during air scan.

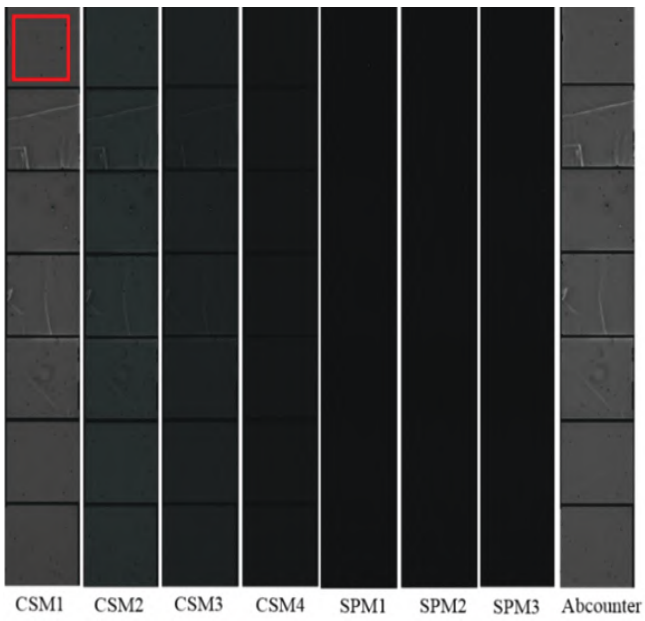

Fig. 6. Reconstructed image of the seven chips MARS camera at different counters. The red rectangular region of interest (ROI) was chosen in each chip to calculate the count in each counter.

2.4 Calculation of Mass Attenuation Coefficient

To analyse the measured data of spectral signature of different materials, the mass attenuation coefficient of different materials was used because it is an energy-specific feature of a material, and therefore is independent of density. The mass attenuation coefficients of material can be extracted from equation (1).

$$\mu = \sum_{m}^{material} \rho_m \left(\frac{\mu}{\rho}\right)_m \quad (1)$$

Where, μ is the linear attenuation of material that can be obtained from reconstructed image of multi-contrast phantom p_m is the concentration or density of **m** as a material of interest and μ/p is the mass attenuation for material of **m**. Linear attenuation and mass attenuation coefficients vary with energy. For lipid and water, which are not the composite materials, their mass attenuation coefficients are easily obtained by substitution of their densities in equation (1). For instance, the mass attenuation of lipid with density of 0.9 g/ml is calculated by equation (2).

$$\mu_{lipid} = 0.9 \times \left(\frac{\mu}{\rho}\right)_{lipid} \quad (2)$$

For the composite materials such as calcium solution, equation (1) is extended as the following equation.

$$\mu = \rho_w \left(\frac{\mu}{\rho}\right)_w + \rho_m \left(\frac{\mu}{\rho}\right)_m \quad (3)$$

$$\begin{aligned} \mu_c &= \rho_w \left(\frac{\mu}{\rho}\right)_w + \rho_m \left(\frac{\mu}{\rho}\right)_m \\ \mu_w &= \rho_w \left(\frac{\mu}{\rho}\right)_w + 0. \times \left(\frac{\mu}{\rho}\right)_m \end{aligned} \quad (4)$$

Where **w** denotes water and μ_c denotes the composite attenuation which includes water used for making a solution. In a multi-contrast phantom, several concentration of the composite materials are typically used. For each concentration of a composite, a system of equations can be formulated equation (4). Where p_m is the known concentration for the material such as calcium or gold in the solution, and this parameter is zero which is representing pure water [14].

The mass attenuation coefficients of a composite material with different concentrations are calculated by solving the over determined system of equations and finding the regression average of the system. For instance, the following equation represents the linear system for the mass attenuation coefficient of gold in a given energy bin.

$$\begin{pmatrix} \rho_{gold1} \\ \rho_{gold2} \end{pmatrix} \left(\frac{\mu}{\rho}\right)_{gold} = \begin{pmatrix} \mu_{gold1} - \mu_{water} \\ \mu_{gold2} - \mu_{water} \end{pmatrix} \quad (5)$$

2.5 Inverse Problem

An inverse problem is defined as the process of calculating the casual factors that produced measurements variations. The inverse problem will use a model to reconstruct an input from the corresponding output. It is called an inverse problem because it starts with the results and then calculates the causes. Algebraic Reconstruction Techniques (ART) are a type of mathematical iterative algorithm used to reconstruct objects from the projection images. Algebraic reconstruction techniques are becoming useful with the advantage of computer technology over the last decade. The advantage of using ART is that they are capable of producing better reconstruction than filtered back projection [15-16].

ART starts with formulating the problem by a system of linear equations, which are defined by the

discrete version of equation (6).

$$P(r\theta) = \sum_{v} \mu_v l_v \quad (6)$$

Where v is the voxel index and l_v is the path-length of the projection ray passing through voxel. This can be written as a linear matrix equation of the form

$$Ax = b \quad (7)$$

Where A is the matrix of path length coefficients, x is a vector containing the linear attenuation coefficients to be reconstructed, and b is the vector containing the projection data.

There are different factors in spectral CT that can impact the solution of ART. These include threshold drifting, detector instability, geometric misalignment, statistical noise and beam hardening. The reconstructed images obtained on several MARS scanner affected by these types of distortion that produce measurement variation.

If an experimental noise ε from threshold drifting, statistical noise, and beam hardening, etc is added up to b term and the sample preparation uncertainty (E) is added up to A, then equation (7) become

$$(b + \varepsilon) = (A + E)x \quad (8)$$

Equation (8) can be rewritten as

$$x = (A + E)^{-1} b + Noiseterm \quad (9)$$

The mass attenuation coefficient of composite materials can be expressed as in linear matrix form

$$\begin{bmatrix} \left(\frac{\mu}{\rho}\right)_{ca} \\ \left(\frac{\mu}{\rho}\right)_{w} \end{bmatrix} = \left(\begin{bmatrix} \rho_{ca}^{1} & \rho_{w}^{1} \\ \rho_{ca}^{2} & \rho_{w}^{2} \end{bmatrix} \right)^{-1} \begin{bmatrix} \mu_{ca}^{conc1} \\ \mu_{w}^{conc2} \end{bmatrix} \quad (10)$$

Where, $x = \begin{bmatrix} \left(\frac{\mu}{\rho}\right)_{ca} \\ \left(\frac{\mu}{\rho}\right)_{w} \end{bmatrix}$, $A^{-1} = \left(\begin{bmatrix} \rho_{ca}^{1} & \rho_{w}^{1} \\ \rho_{ca}^{2} & \rho_{w}^{2} \end{bmatrix} \right)^{-1}$ and $b = \begin{bmatrix} \mu_{ca}^{conc1} \\ \mu_{w}^{conc2} \end{bmatrix}$

Therefore, small noise in the forward form of equations (9) and (10) is magnified in the inverse form in which A^{-1} maps b to x. This is called “inverse noise amplification" and it becomes more significant when a composite material is used because it involves the all sources of noise that were mentioned above for each component. The K-edge imaging is an important application using spectral CT scanner. The detectability of K-edge property of different materials depends on the accurate energy threshold setting. For K-edge imaging, threshold settings for energy bins on both sides of a K-edge have a major impact on spectral image quality in terms of image contrast and noise level [17]. In case of K-edge imaging small changes in threshold drifting results in a large change in reconstructed images that can be produce measurement variation in spectral CT scanner.

4. Results

4.1 Attenuation Variation

This section illustrated the result of intra and inter-scan variability of measured mass attenuation coefficient during repeated scans of the multi-contrast phantom. Fig. 7 displays the mass attenuation profile of different materials at different energy bins for different scans that clearly appeared significant variation in their spectral signature. The variation of the mass attenuation coefficients between different scans was assessed by relative standard error (RSE). Fig. 8 illustrates the intra-scan measurement variation of mass attenuation of different materials in different energy bins. Gold, gadolinium, iodine, calcium shows a higher variation of RSE than lipid and water and significant variation has appeared in the higher energy bins. Fig. 9 represents the inter-scan measurement variation of mass attenuation of different materials in different energy bins in each scan. In the case of gadolinium, all measurements in each scan has a significant variation. While lipid and water have the same RSE value across all scans and in each energy bins. The Bland-Altman (BA) method was applied to evaluate the proportional bias between different measurements. Linear attenuation coefficients of each voxel were calculated corresponding to ROI for 8 mg/mL gold, gadolinium, and 18 mg/mL iodine, lipid, and water at lower energy bin to produce the (BA) plot. The linear attenuation difference of each voxel between two back-to-back scans was plotted against the average linear attenuation of two scans. Fig. 10 and Fig. 11 represent the Bland-Altman (BA) plot between two measurements (scans) of composite and single materials at lower energy bins. It is clear that there are some points that are outside the limit of agreement in case of composite materials while fewer points outside the limit of agreement in case of single materials. All measurement points of composite materials are less concentrated in the middle of the mean than single materials. From the point of the limit of agreement, this indicates that all composite materials have higher measurement instability than lipids and water.

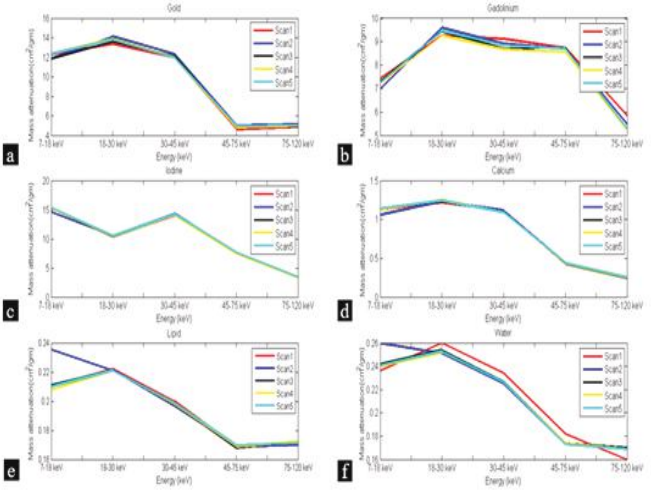

Fig. 7. Mass attenuation profiles (a) for gold (b) for gadolinium (c) for iodine (d) for calcium (e) lipid and (f) for water that used multi-contrast phantom with CZT-Medipix3RX detector at different energy bins of repeated scans. Mass attenuation value of lipid and water in scan-2 is slightly higher at 7-18 KeV but scan-1 is far from than other scans in case of water.

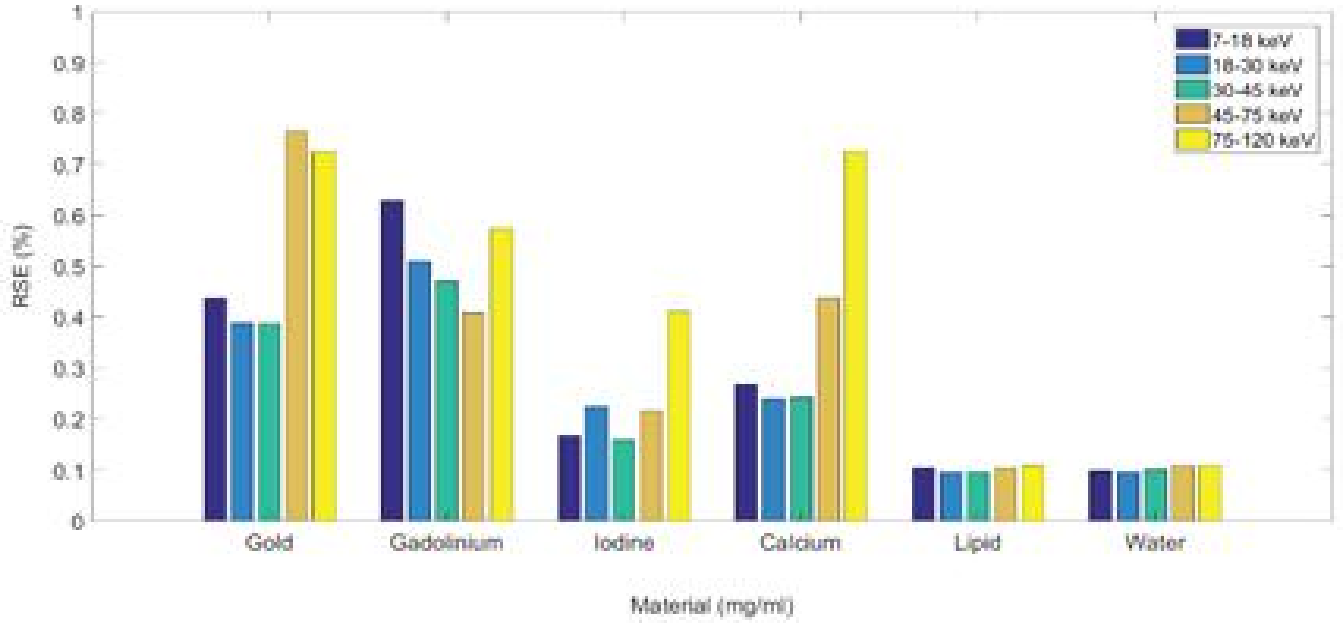

Fig. 8. The intra-scan variation of mass attenuation coefficient of different materials at different energy bins within any particular scan. Fourth and fifth energy bins show the higher value of RSE of gold, gadolinium, iodine, and calcium than lipid and water.

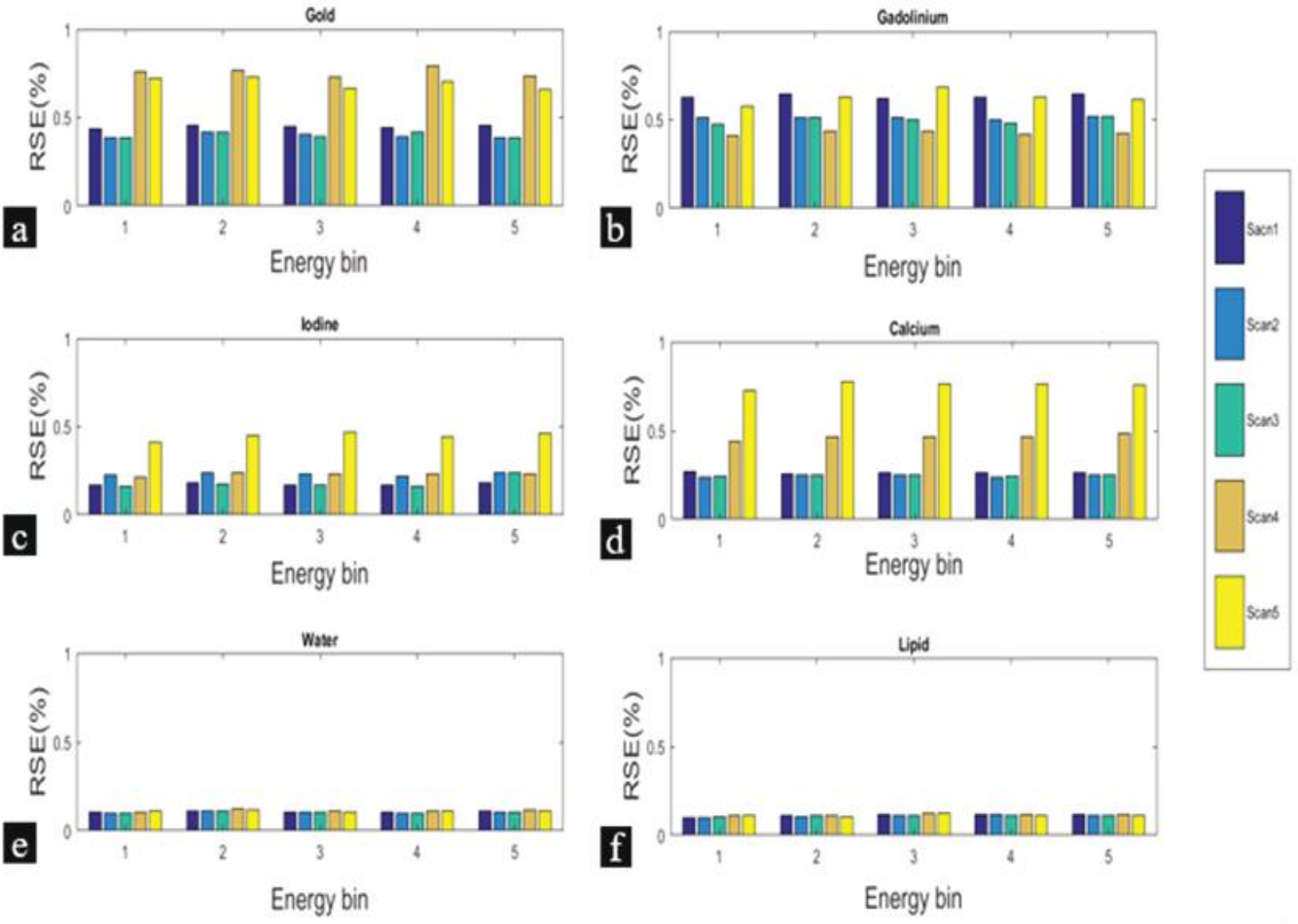

Fig. 9. Inter-scan variation of mass attenuation profiles (a) for gold (b) for gadolinium (c) for iodine (d) for calcium (e) for water and (f) for lipid.

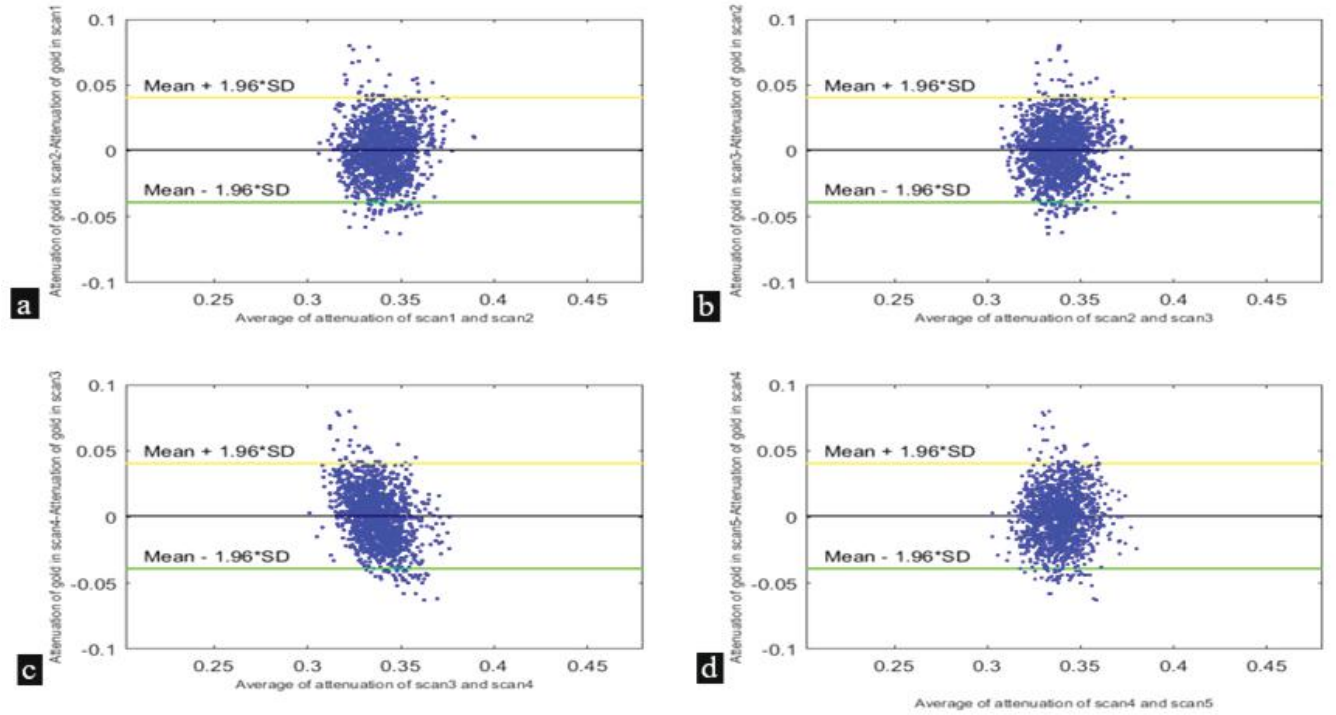

Fig. 10. Bland-Altman plot of composite material such as gold (a) for scan 1 and scan 2 (b) for scan 2 and scan 3 (c) for scan 3 and scan 4 (d) for scan 4 and scan 5 at lower energy bin. There are significant measurement points outside the limit of agreement.

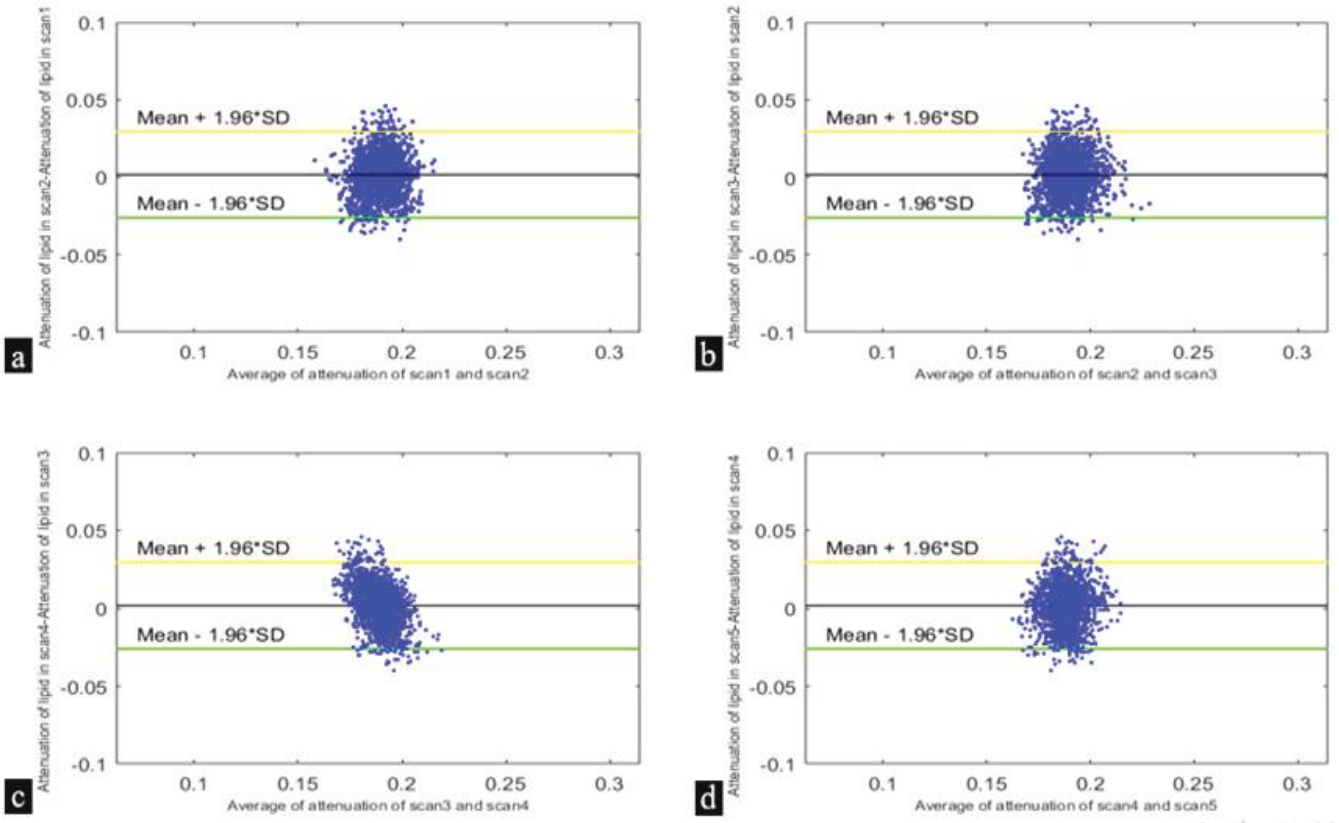

Fig. 11. Bland-Altman plot of single material such as lipid (a) for scan 1 and scan 2 (b) for scan 2 and scan 3 (c) for scan 3 and scan 4 (d) for scan 4 and scan 5 at lower energy bin. There are significant measurement points outside the limit of agreement.

4.2 Count Variation

Count rate performance of Medipix3RX detector was investigated during air scan to see temporal stability in MARS scanner. The results of this experiment show the inter-scan count variation across the total number of the frame of the raw image. Fig. 12 shows the results of the relative count variation in different chips of an air scans. It is clear that chip 4 shows the higher value of relative count in counter1, counter2, and counter3. The relative count of each (CSM) counter was measured with respect to the arbitration counter. The measured relative count rate was averaged over a selected region of interest of a chip with 110 pixels across the total number of the frame.

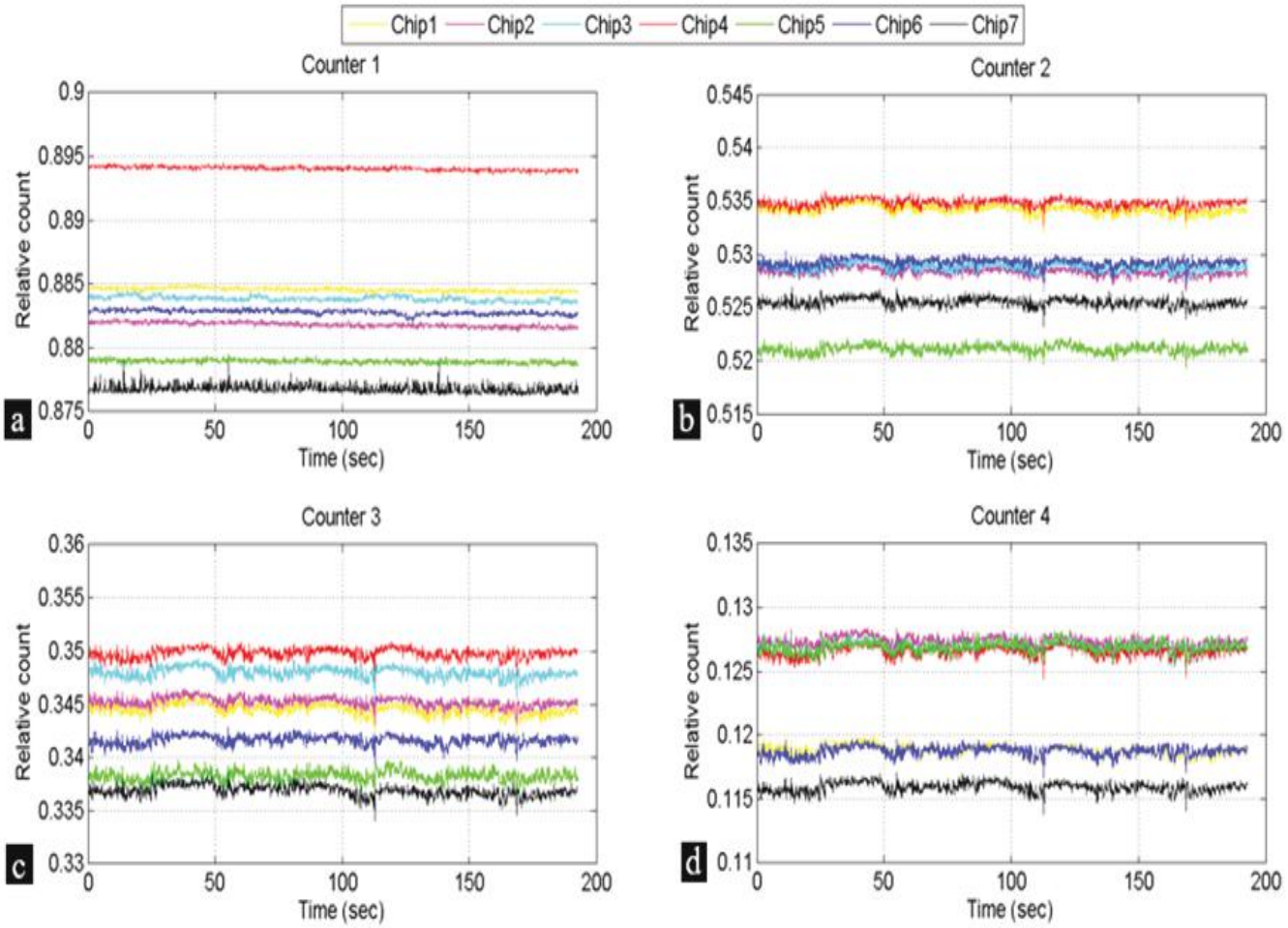

Fig. 12. The relative count rate of the different (CSM) counters (a) first charge summing counter (b) second charge summing counter (c) third charge summing counter (d) fourth charge summing counter with respect to arbitration counter in each chip during the initial scan.

Fig. 13 represents the inter-scan variation of relative count in different counter in each scan. This result is shown to see the temporal count variation in different counters with respect to the arbitration counter. If the kVp is stable but the count of each CSM counter with respect to the arbitration counter changes over time then it indicates threshold drifting may exist. From this figures, it is clear that the relative count of each counter changes in each scans and indicating the existence of threshold drifting.

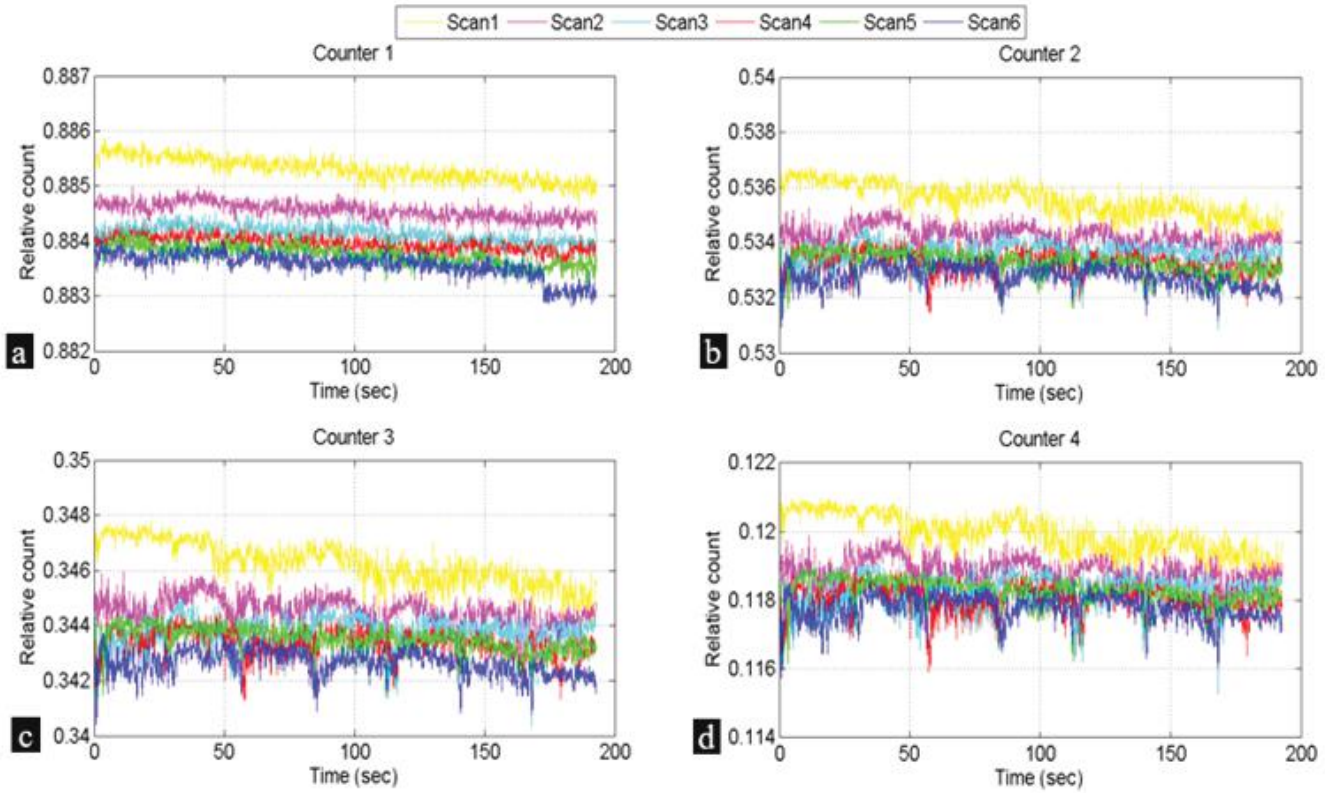

Fig. 13. The relative count in each scan of the different counter (a) first charge summing counter (b) second charge summing counter (c) third charge summing counter (d) fourth charge summing counter. The variation in the ASIC temperature could be the possible reason for the variation in counts with time.

5. Discussion

This work demonstrates the characterization of measurement stability in the spectral CT scanner using the Medipix3RX photon-counting detector. A study was conducted to assess intra and inter-scan measurement variation in the mass attenuation profile of different materials. The variation of mass attenuation coefficient was assessed by the relative standard error. In general, the results of the study show that the mass attenuation coefficients of lipid and water have fewer variations as compared to calcium, gadolinium, iodine, and gold. A hypothesis was made to assume how spectral signature is being distorted by different experimental noise. For the composite materials, the measurement of the mass attenuation profile might be influenced by the inverse noise amplification as compared to the single materials. The noise involved in the calculation of mass attenuation coefficients originates from the uncertainties of the scan measurements, inaccurate threshold setting between the K-edge, geometric misalignment, etc. The uncertainties of the measurements include statistical noise, beam hardening, the artifact from material reconstruction algorithms, output variation of the x-ray source, and energy threshold drifting in the detector. The superposition of such uncertainties from each material in a solution such as water and gold caused a higher variation of mass attenuation coefficient in a composite material than water or lipid.

The higher variation of the K-edge materials is thought to be due to energy threshold drifting. In the worst-case scenario, the K-edge may be captured in the adjacent energy bin which is more likely when a large threshold variation exists in the detector's channel. In general, all high-Z materials have significant K-edge properties and therefore, are sensitive to select appropriate energy threshold above or below the K-edge. The K-edge image contrast with spectral CT depends on the specifications of the two energy bins on both sides of a K-edge in the attenuation profile of a relatively high atomic number material. [18] The miss-adjustment of energy threshold especially for K-edge materials might lead to inverse noise amplification that produces significant measurement error in case of all K-edge materials. The

temperature effect is also one of the effective parameters on the measurement variation which needs more investigation in the future.

The variability of relative count of each charge summing mode was evaluated across the total number of the frame with respect to the arbitration counter to investigate the threshold drifting during the air scan. The temporal stability of the Medipix3RX chip was observed by measuring the count rate capability of each chip. The reason for doing this investigation is to see the temporal count variation in each chip and investigate count information in each counter. It was noticed that there exists a significant fluctuation of the measured relative count in each chip at the different scan. The relative count rate in each counter is decreased by increasing the number of back-to-back air scans that indicate that temporal count variation exists in each chip which shown in Fig. 14. The variation of temperature in the application-specific integrated circuit (ASIC) during the first 7-10 minutes could be the possible reason for the variation in counts with time. It is also expected that such temperature rises could change the energy threshold for each counter and which ultimately changes the energy response of the detector. The relative count variation over time shows that the energy threshold is not stable and further work needs to be done to eliminate this instability. It can be seen in Fig. 12 there is a high degree of correlation between ASIC and energy thresholds e.g. the count spikes occurs simultaneously in each plot. Sources of variation consistent with this pattern include x-ray flux variation, bias voltage variation, and common mode electronic noise affecting the ASIC analogue circuits. The difference in relative counts between chips is greater than the temporal variation for a single chip. This suggests it may be possible to improve energy calibration using this type of measurements. Zuber *et al.* [19] explained that the overall count rate fluctuation is a function of temperature instability of the spectral CT scanner. The temperature fluctuations most probably induce a shift in the effective threshold position. The photon-counting detector is currently subject to various effects that limit its count rate capability. In general, all these effects arise either from the sensor or from the ASIC and further work needs to be done in the future.

6. Conclusions

The presented work in this paper demonstrates a pilot study to evaluate the stability in repeated measurements over time to investigate the sources of variability in MARS spectral CT scanner. The inter-scan and intra-scan variability of measured mass attenuation were evaluated using several composite and single materials and it was found that the measurement variation was more likely for composite materials such as gold, gadolinium, and iodine this is due to the inverse noise amplification that occurs with these materials. The stability of the Medipix 3RX photon counting detector in the MARS scanner was also evaluated by measuring the relative count. These investigations provide useful insights into the source of variation of spectral CT system and indicate potential areas where future improvements in performance may be made.

Acknowledgement:

The author's world like to thanks the University of Canterbury Christchurch, MARS Bioimaging Ltd., University Otago, Christchurch and Medipix collaborations at CERN for supporting this reserach.

References

1. McCollough CH , Leng S, Yu L, Fletcher JG; Dual- and multi-energy CT, principles, technical approaches, and clinical applications, Radiology, 276(3): 637-53 (2015).
2. Doesburg RM; The MARS photon processing cameras for spectral CT, PhD thesis, Christchurch, New Zealand, University of Canterbury, 2012.
3. Ballabriga R, Campbell M, Greiffenberg D, Erik HM, Llopart X, Plackett R, *et al.;* Characterization of the medipix3 pixel readout chip, J. Inst., 6 (1): C01052 (2011).
4. Ronaldson JP; Quantitative soft tissue imaging by spectral CT with medipix3, PhD thesis, Christchurch, New Zealand, University of Otago, 2012.
5. Younis RA; Using MARS spectral CT for identifying biomedical nanoparticles, PhD thesis, Christchurch, New Zealand, University of Canterbury, 2013.
6. Anderson NG, Butler AP; Clinical application of spectral molecular imaging, potential and challenges, contrast media & molecular imaging, 9(1): 3-12 (2014).
7. World's first ever colour x-ray performed on a human; https://www.news18.com/news/lifestyle/health-and-fitness-worlds-first-ever-colour-x-ray-performed-on-a-human-1810229.htm.
8. Atharifard A, Healy JL, Goulter BP, Ramyar M, Vanden Broeke L, Walsh MF *et al.*; Per-pixel energy calibration of photon counting detectors, J. Instr., 12(3): C03085 (2017).
9. Uddin R; Spectral image quality in MARS scanners, PhD thesis, Christuchurch, New Zealand, University of Canterbury, 2019.
10. Shamshad M; Characterization of x-ray source and camera in

MARS spectral system, PhD thesis, Christuchurch, New Zealand, University of Otago, 2016.

11. Kobayashi T, Ogawa K; Accuracy of linear attenuation coefficients measured with a photon counting CT system, Nuclear Science Symposium and Medical Imaging Conference (NSS/MIC) 2012.
12. Curtis TE, Roeder RK; Quantification of multiple mixed contrast and tissue compositions using photon-counting spectral computed tomography, J. Med. Imaging, 6(1): 013501 (2019).
13. Persson M, Bornefalk H; A framework for evaluating threshold variation compensation methods in photon counting spectral CT, IEEE Trans. Med. Imaging, 31(10):1861-74 (2012).
14. Rajendran K; MARS spectral CT technology for orthopaedic applications, PhD thesis, Christuchurch, New Zealand, University of Otago, 2015.
15. Gordon R, Bender R, Herman GT; Algebraic reconstruction techniques (ART) for three-dimensional electron microscopy and x-ray photography, J. Theor. Biol. 29: 471-481 (1970).
16. Bateman CJ; Methods for material discrimination in MARS multi-energy CT, PhD thesis, Christuchurch, New Zealand, University of Otago, 2014.
17. He P, Wei B, Cong W, Ge W; Optimization of K-edge imaging with spectral CT, Med. Phys., 39 (11): 6572-79 (2012).
18. He P, Wei B, Feng P, Chen M, Mi D; Material discrimination based on K-edge characteristics, Com. Math. Meth. Medi. 2013 (308520); 1-6 (2013).
19. Zuber M, Hamann E, Ballabriga R; An investigation into the temporal stability of CdTe-based photon counting detectors during spectral micro-CT acquisitions, Biomed. Phys. Eng. Express, 1(2): 025205 (2015).